JOURNAL OF MATERIALS SCIENCE 28 (1993) 4804–4810

Oxygen self-diffusion in rutile under hydrothermal conditions

P. F. DENNIS
Earth Science Research Group, School of Environmental Sciences, University of East Anglia, Norwich NR4 7TJ, UK

R. FREER*
Materials Science Centre, University of Manchester/UMIST, Grosvenor Street, Manchester, M1 7HS, UK

Oxygen self-diffusion coefficients have been determined for synthetic and natural rutile single crystals under hydrothermal conditions at 100 MPa total pressure and in the temperature range 873–1373 K. The diffusion coefficients are lower than the results from dry gas exchange studies would predict. Between 973 and 1373 K the results can be characterized by two linear Arrhenius relationships. $D = 1.14 \times 10^{-11} \exp(-168.8\ \text{kJ mol}^{-1}/RT)\ \text{m}^2\ \text{s}^{-1}$ for the natural rutile, and $D = 2.41 \times 10^{-12} \exp(-172.5\ \text{kJ mol}^{-1}/RT)\ \text{m}^2\ \text{s}^{-1}$ for the synthetic crystal. The results have been interpreted in terms of a defect model involving the dissolution of water in rutile as substitutional hydroxyl defects on oxygen lattice sites, with a solution enthalpy in the range 81–106 kJ mol^{-1}.

1. Introduction

Rutile, TiO_2 has tetragonal symmetry with the titanium ions arranged on a body centred tetragonal sub-lattice and octahedrally co-ordinated by the oxygen ions. In the intrinsic state rutile is an oxygen deficient, *n*-type semiconductor with only small deviations from stoichiometry. Maximum values of x in TiO_{2-x} are close to 0.01; the departure from stoichiometry being a function of both temperature and oxygen fugacity [1, 2]. The type of ionic defects responsible for the non-stoichiometry are still the subject of active debate. Kofstad [2] proposed that the defect structure simultaneously comprises doubly charged oxygen vacancies (using Kroger–Vink notation [3]) $V_O^{\cdot\cdot}$ and interstitial titanium ions with three and four effective charges, $Ti_i^{\cdot\cdot\cdot}$ and $Ti_i^{\cdot\cdot\cdot\cdot}$ respectively. The model predicts that $V_O^{\cdot\cdot}$ dominate at high oxygen fugacities and low temperatures, whereas $Ti_i^{\cdot\cdot\cdot}$ and $Ti_i^{\cdot\cdot\cdot\cdot}$ are the dominant defects towards the lower limit of the non-stoichiometric range, at higher temperatures and lower oxygen fugacities.

Oxygen self-diffusion data are certainly consistent with a transport mechanism involving isolated oxygen vacancies, although results are only available for material in the extrinsic state. The most complete sets of diffusion data are those of Haul and Dumbgen [4, 5] and Haul *et al.* [6]. Their results, determined using bulk ^{18}O isotope exchange techniques for TiO_2 powders annealed in O_2, are well described by a single Arrhenius relationship covering the temperature range 983–1573 K

$$D_{ox} = 1.0 \times 10^{-7} \exp(-251 \pm 6\ \text{kJ mol}^{-1}/RT)\ \text{m}^2\ \text{s}^{-1} \quad (1)$$

Subsequent single crystal exchange experiments analysed by ^{18}O isotope tracer profiling methods (proton activation [7, 8] and secondary ion mass spectrometry, SIMS [9]) yielded results that are substantially in agreement with this relationship. These studies have also demonstrated the existence of a small diffusion anisotropy with transport perpendicular to the *c*-axis being approximately 50% faster than that parallel to the *c*-axis at 1620 K [5] and 1353 K [9]. Furthermore, Haul and Dumbgen [4] observed no dependence of oxygen diffusivity on oxygen fugacity within the range 10^5 to 1.3×10^{-1} Pa at 1170 K. This latter result is consistent with extrinsic diffusion behaviour. The high Al_2O_3 content (100–200 p.p.m.) of the samples used by Haul and Dumbgen suggests an impurity-controlled, vacancy diffusion mechanism. Oxygen vacancies are introduced by the reaction

$$Al_2O_3 = 2Al_{Ti}^{\cdot} + V_O^{\cdot\cdot} + 3O_O^{x} \quad (2)$$

This simple interpretation of the data is supported by the study of Arita *et al.* [9], who found that D_{OX} was faster in rutile doped with Cr_2O_3.

A very interesting, preliminary set of diffusion anneals were carried out in water-saturated air by Haul and Dumbgen [5]. At both 1088 and 1170 K the oxygen self-diffusion coefficients were slightly lower

* Author to whom correspondence should be addressed.

0022–2461

than those obtained in experiments performed in dry oxygen by a factor of almost two. The cause of the reduction is not understood, though Haul and Dumbgen suggested that water dissolves in rutile according to the reaction:

$$O_O^x + V_O^{\cdot\cdot} + H_2O = 2OH_O^{\cdot} \quad (3)$$

The effect of incorporating hydroxyl defects is to reduce the oxygen vacancy concentration and thus the oxygen self-diffusion coefficient. Infrared spectroscopic studies indicate that the dominant hydrogen speciation in rutile is as OH^- [10, 11]. At significantly higher water activities ($\cong$ 100 MPa) and 1323 K, Freer and Dennis [12] obtained an oxygen diffusion coefficient of $3.2 \times 10^{-19}\,m^2\,s^{-1}$ for natural rutile crystal. This is slower by a factor of approximately 100 than the results of dry oxygen gas exchange experiments would predict [4–9]. This observation is qualitatively consistent with Equation 3 in the sense that increasing the water activity should lead to a further reduction in the oxygen vacancy concentration. However, our understanding of the role of water in the defect structure of rutile, and other oxides, is too limited to uniquely define this as the correct model.

To contribute to a better understanding of the diffusion mechanism in rutile, and the role of water-related defects, oxygen self-diffusion coefficients in rutile have been determined as a function of temperature (873–1373 K) under hydrothermal conditions at 100 MPa total pressure. The crystals used, one synthetic and one natural, had widely differing impurity concentrations to test the effect, if any, of aliovalent dopants on the incorporation of water related defects. Prepared fragments from the two crystals were employed in isotope exchange experiments with water enriched in ^{18}O; the tracer diffusion profiles were subsequently determined using SIMS. Preliminary results for the synthetic rutile were reported in an earlier note [13] but are included here with the new data for the natural crystal for the sake of completeness and comparison.

2. Experimental procedure

2.1. Samples and sample preparation

The samples used in this study were prepared from larger natural and synthetic crystals. The natural sample, from Minas Gerais, Brazil, was a well developed needle approximately 7 mm long. Electron microprobe EDS analysis of representative crystals from the same source show a variable impurity content with average concentrations for the main impurities as follows: Si (2170/10^6 Ti); Fe (2700/10^6 Ti); Mg (750/10^6 Ti). No information is available for the minor trace constituents. The synthetic crystal, a colourless, transparent plate (approximately $10 \times 4 \times 1$ mm), was cut from a boule grown by Dr D. Jones of the Centre for Materials Science, Birmingham University. The principal impurity contents are: Si (1320/10^6Ti); Mg (400/10^6 Ti); Al (160/10^6 Ti); Fe (100/10^6 Ti).

Small pieces ($2 \times 2 \times 1$ mm) were cut from both crystals, with the large faces oriented perpendicular to the c-axis. These were then polished using SiC and diamond paste down to < 1 μm finish.

2.2. Hydrothermal isotope exchange experiments

Charges for the diffusion experiments consisted of a crystal fragment sealed with approximately 9 mg of water enriched in ^{18}O ($^{18}O/(^{18}O + {}^{16}O) \cong 40\%$) in 3 mm outside diameter Pt tubes. The capsules were run in internally heated, gas medium pressure vessels at temperatures to 1373 K and at a pressure of 100 MPa. Two charges were run at each temperature: one containing a natural crystal and the other a synthetic crystal. Anneal durations ranged from approximately 23 h at 1373 K to 70 h at 873 K.

A summary of the run conditions is given in Table I. The oxygen fugacity of all the runs is thought to be close to the natural Ni–NiO buffer of the pressure vessels. The water fugacity is close to 100 MPa for all runs (Table I). Heating and cooling periods from 100 °C below the desired run temperatures were less than 1% of the total anneal durations. Reported temperatures are believed to be accurate to $\pm$ 5 °C, the pressure to $\pm$ 5 MPa. At the termination of the run the charges were checked for leaks and the presence of excess water in the capsules.

2.3. SIMS analysis

The oxygen isotope composition as a function of

TABLE I Summary of experimental conditions and results

Sample	T (°C)	log f(H_2O) (Pa)	log f(O_2) (MPa)	t ($\times 10^{-5}$ s)	d (μm)	D ($m^2\,s^{-1}$)
OX106A	600	7.81	− 14.14	3.2154		$< 2.5 \times 10^{-22}$
OX104A	700	7.87	− 11.21	2.5290	0.34 ± 0.05	1.18×10^{-20}
OX109A	800	7.93	− 8.83	2.5368	0.57 ± 0.05	5.28×10^{-20}
OX107A	900	7.96	− 6.85	2.3754	1.50 ± 0.20	4.09×10^{-19}
OX105A	1000	7.97	− 5.19	1.5384	2.15 ± 0.05	1.02×10^{-18}
OX108A	1100	7.98	− 3.76	0.8160	3.35 ± 0.05	5.41×10^{-18}
OX106B	600	7.81	− 14.14	3.2154	failed run	failed run
OX104B	700	7.87	− 11.21	2.5290	0.34 ± 0.02	1.49×10^{-21}
OX109B	800	7.93	− 8.83	2.5368	0.35 ± 0.05	9.40×10^{-21}
OX107B	900	7.96	− 6.85	2.3754	0.72 ± 0.05	4.50×10^{-20}
OX105B	1000	7.97	− 5.19	1.5384	0.85 ± 0.03	1.64×10^{-19}
OX108B	1100	7.98	− 3.76	0.8160	1.145 ± 0.005	8.52×10^{-19}

depth beneath the sample surface was determined by SIMS ion-microprobe analysis. The instrument used in this study was an Atomika A-DIDA II quadrupole equipped ion-microprobe [14]. Full details of the technique are given in Freer and Dennis [12] and Dennis [15].

To obtain a good electrical contact between the semiconducting rutile and the sample holder the crystals were fixed, using silver dag, onto Pt foil sample mounts. SIMS operating parameters during the analyses were as follows: the primary ion beam was mass filtered $^{40}Ar^{+}$, accelerated to 10 keV, with a maximum current of 150 nA focussed into a 50 μm spot at the sample surface. To ensure flat bottomed craters and improve depth resolution by eliminating contributions from the crater edge to the determined profiles, the beam was rastered over an area of up to 350×350 μm, with the data acquisition electronics gated to accept secondary ions from the central 18% of the crater floor. Depending on the size of the rastered area, sputter rates ranged from 0.8 nm s^{-1} to 0.15 nm s^{-1}.

Charge compensation of the primary ion beam was achieved using an electron flood gun operated at 250–500 eV energy and 10–20 mA total current.

Negative secondary ions at m/e equal to 16, 18 and 47, corresponding to the species $^{16}O^{-}$, $^{18}O^{-}$ and $^{47}Ti^{-}$, were sequentially monitored by rapid peak switching. Count rates for the total oxygen signal exceeded 1×10^5 c.p.s. and integration periods for each species were 2 s. No corrections were made to the raw data, with maximum background count rates less than 10 c.p.s. Oxygen-18 isotope abundances recorded in the tails of the diffusion profiles and on unexchanged samples were 0.2%, in agreement with the natural abundance for ^{18}O.

The sputtered craters were examined optically using interference contrast reflected light, and their depths measured using a Talystep. The determined crater depths, with one exception (OX107A) are accurate to $\pm$ 0.05 μm or better (Table I).

2.4. Computation of diffusion coefficients

In the experiments, self-diffusion of the oxygen isotope may be modelled by transport into a semi-infinite medium from a fluid phase held at a constant isotopic composition. The surface concentration of ^{18}O in the crystals always closely approached that of the initial starting fluid ($^{18}O/(^{18}O + {}^{16}O) \cong 40\%$), indicating a rapid phase boundary exchange reaction for the fluid–solid transfer of oxygen.

The general solution to Fick's second law under these boundary conditions is given by [16]

$$\frac{C_x - C_1}{C_O - C_1} = \text{erfc}\,\frac{X}{(Dt)^{1/2}} \qquad (4)$$

where C_x, C_O and C_1 are, respectively, the ^{18}O concentration at a distance X from the crystal surface, in the fluid phase and at $X = \infty$ in the crystal ($\cong 0.002$, the natural composition), t is the hydrothermal anneal time, D is the diffusion coefficient and erfc is the error function compliment.

Plots of $\text{erfc}^{-1}[(C_x - C_1)/(C_O - C_1)]$ versus X give a straight line with a slope equal to $1/(Dt)^{1/2}$. An example of a measured diffusion profile and the transformed data is given in Fig. 1 (a) and (b) for run OX108A (annealed at 1373 K for 73 min).

2.5. Error analysis

The precision of the results was esimated by considering the uncorrelated errors due to the isotope exchange anneal and SIMS anlysis [15]. The diffusion coefficients are determined from an equation of the form

$$D = p^{-2}t^{-1} \qquad (5)$$

where p represents the slope of the erfc^{-1} versus depth (X) plot and t is the isotope exchange anneal duration.

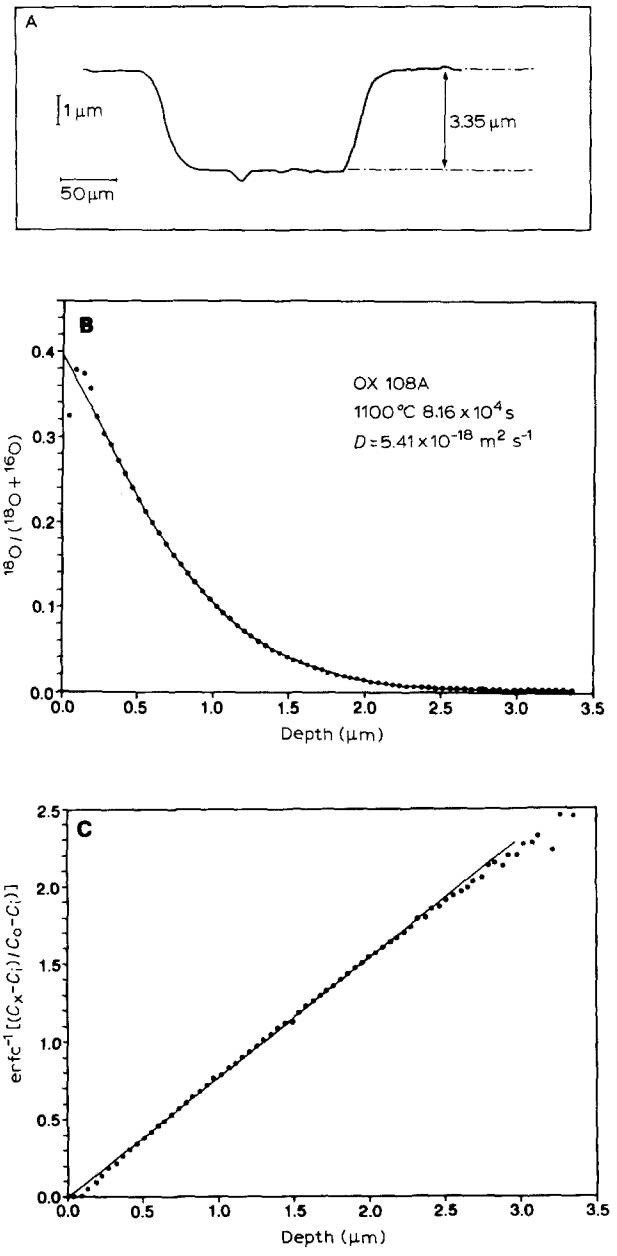

Figure 1 Sample OX108A: (A) Talystep profile of the SIMS sputter eroded crater; (B) The concentration profile of ^{18}O as a function of depth. The measured isotope ratios are shown by the open symbols and the solid line represents the best fit to the data determined using the inverse error function, plot (C) — see text for details.

Accordingly the relative precision of D, $\delta D/D$ is given by

$$\frac{\delta D}{D} = \left(\left(\frac{2\delta p}{p}\right)^2 + \left(\frac{\delta t}{t}\right)^2\right)^{1/2} \quad (6)$$

The error in the anneal duration, δt, was always less than 1% of t and therefore was ignored. The maximum error in p was estimated from the precision of the crater depth measurements. In the worst cases, which were generally for the shortest profiles, the crater depths were measured to a precision of approximately $\pm$ 15%. Using the value for $\delta p/p$ in Equation 6 gives a relative precision, $\delta D/D$, for the diffusion coefficient of approximately $\pm$ 0.3 (i.e. $\pm$ 30%).

In addition to the random errors, the accuracy of the results may be affected by ion bombardment-induced modification of the measured diffusion profiles during the SIMS analysis. Two effects may be important: (i) knock-on or recoil phenomena [17], including radiation enhanced diffusion; (ii) the generation and amplification of surface topography. These processes will lead to some broadening of the tracer diffusion profiles, though it is difficult to quantify the magnitude of the effect. Unpublished results by Dennis indicate that errors due to the knock-on related phenomena may be negligible. Analysis of a step function distribution of ^{18}O in anodically oxidised Ta_2O_5, using 10.6 keV Ar^+ primary ions, indicates a maximum broadening of 7–10 nm.

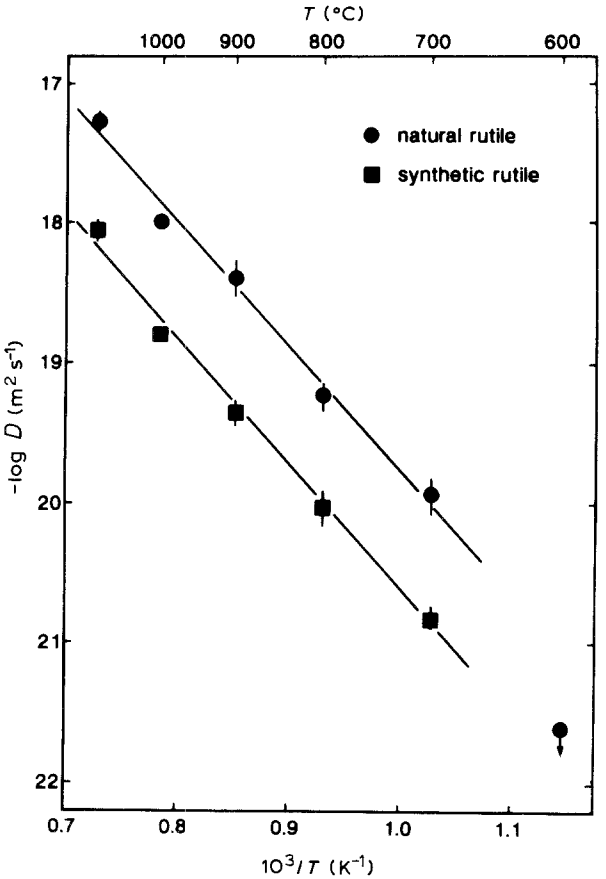

Figure 2 Log D_{ox} as a function of reciprocal temperature for natural and synthetic rutile. The solid lines represent a least squares fit to the data in the temperature interval 700–1100 °C. Values for the activation parameters are given in the text.

The effect of original surface topography and its further amplification during sputtering is more difficult to assess. However, all the samples, except OX107A, exhibited relatively smooth bottomed craters to within the accuracy of the Talystep measurement. Moreover, with the exception of occasional light etching of polish-related damage, the original polished faces remain undamaged during the diffusion anneal. For these samples, therefore, it is concluded that any surface roughness effects may be neglected. In contrast, sample OX107A showed a significant degree of surface roughness, with an amplitude of 0.5 μm on the floor of the crater. This is reflected in the poor precision of the depth measurement (Table I). The roughness is due to a significant striation that developed during the high temperature anneal. The degree to which this roughness contributes to a systematic inaccuracy in the determined diffusion coefficient for this sample is not known, although it is not thought to be greater than the quoted precision of $\pm$ 30%.

3. Results

Oxygen-18 tracer diffusion coefficients for rutile are listed with a summary of the experimental conditions in Table I. The values of D_{ox} are plotted against reciprocal absolute temperature in Fig. 2. In the temperature range 973–1373 K the results are well described by standard Arrhenius relationships, with diffusion rates in natural rutile faster than in synthetic rutile by approximately one order of magnitude. For the natural rutile

$$D_{ox} = 1.14^{+9.77}_{-1.02} \times 10^{-11} \times \exp(-168.8 \pm 32.9\ \text{kJ mol}^{-1}/RT)\ \text{m}^2\,\text{s}^{-1} \quad (7)$$

and for the synthetic rutile

$$D_{ox} = 2.41^{+9.73}_{-1.93} \times 10^{-12} \times \exp(-172.5 \pm 23.6\ \text{kJ mol}^{-1}/RT)\ \text{m}^2\,\text{s}^{-1} \quad (8)$$

where R is the gas constant (8.314 J K^{-1} mol^{-1}) and T is the absolute temperature. The errors are quoted at the 90% confidence level.

Two experiments were carried out at 873 K, OX106A and OX106B, corresponding to the natural and synthetic rutile, respectively. The tracer diffusion profiles in these samples were too short to analyse with any degree of precision and it is only possible to give an upper estimate to the diffusion coefficient for sample OX106A (Table I). This estimate, $< 2.5 \times 10^{-22}$ m^2 s^{-1}, is a factor of approximately 10 lower than results extrapolated from high temperatures would predict (Fig. 2).

4. Discussion

4.1. Comparison with other data

A clear difference exists between the present results, determined under hydrothermal conditions, and those of previous studies which were all carried out in pure O_2 at fugacities in the range 3×10^{-1}–10^5 Pa [4–9].

All these results are shown in the compilation Arrhenius diagram (Fig. 3), where a marked reduction in the oxygen diffusivity is observed for rutile annealed in water at moderate to high pressures (100 MPa) and at temperatures greater than 873–973 K. For example, at 1373 K the oxygen self-diffusion coefficient is slower by a factor of 20–100, depending on the sample, than the dry gas results at the same temperature. This result confirms the preliminary data of Haul and Dumbgen [5], who noted a small decrease in D_{OX} (by a factor < 2) on annealing TiO_2 in water-saturated air at 1088 and 1170 K. In the only other study that has been carried out under hydrous conditions, Freer and Dennis [12] reported an oxygen diffusivity of $3.2 \times 10^{-19}\,m^2\,s^{-1}$ at 1323 K and 100 MPa P_{H_2O} for a different natural crystal to that used in this study. This value is in good agreement with our new data.

In the temperature range 983–1673 K the activation enthalpies, ΔH, for oxygen self-diffusion in rutile under dry O_2 conditions are all in good agreement and lie between 251 and 276 kJ mol^{-1} [5, 7–9]. The pre-exponential constants, D_O, and hence the absolute magnitudes of the reported diffusion coefficients are also in good agreement (Fig. 3). Slight variations in the results, if significant, may be due to the different impurity contents of the samples. For example, Arita *et al.* [9] reported an increase in D_{OX} after doping a sample with 0.08 mol% Cr_2O_3. Whilst there have been no systematic studies of the effect of oxygen fugacity on the activation parameters, Haul and Dumgen found no change in D_{OX} with oxygen fugacity between 10^5 and 1.3×10^{-1} Pa at 1170 K.

In contrast to the dry gas studies, ΔH for oxygen self-diffusion under hydrothermal conditions is significantly reduced to approximately 170 kJ mol^{-1} (equations 7 and 8 and Figs 2 and 3). Moreover, the pre-exponential constants for both the natural and synthetic rutile are also greatly reduced, c.f. Equation 1 with Equations 7 and 8.

Because of the lower ΔH and D_O values for oxygen diffusion under hydrothermal conditions, the present results approach the extrapolated dry gas data at temperatures in the range 873–973 K (Fig. 3). It is not clear, however, whether the two sets of data cross over, such that at lower temperatures the oxygen self-diffusivity is faster under hydrothermal conditions than dry O_2 conditions. The single result obtained at 873 K is more consistent with the extrapolated high temperature dry gas data and suggests that there may be a transition between the two sets of results rather than a cross-over.

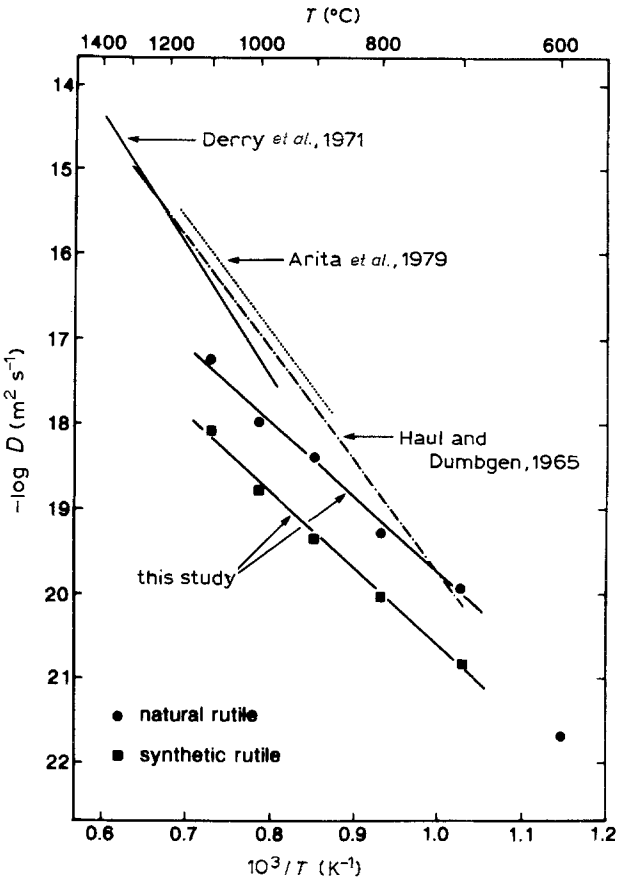

Figure 3 Complication Arrhenius diagram for the available oxygen self diffusion data in rutile.

4.2. Defect chemistry

The dominant disorder in rutile is still under active discussion. On the basis of the available thermogravimetric data, Kofstad [2] proposed that the defect structure simultaneously comprises doubly charged oxygen vacancies, $V_O^{\cdot\cdot}$, and interstitial titanium ions with three and four effective charges, $Ti_i^{\cdot\cdot\cdot}$ and $Ti_i^{\cdot\cdot\cdot\cdot}$, respectively. The model predicts that $V_O^{\cdot\cdot}$ predominate at high oxygen fugacities and low temperatures, whereas $Ti_i^{\cdot\cdot\cdot}$ and $Ti_i^{\cdot\cdot\cdot\cdot}$ are the dominant defects toward the lower limit of the stoichiometric range, at higher temperatures and lower oxygen fugacities. Certainly, experimental data do indicate that in rutile approaching compositions of $TiO_{1.99}$ interstitial titaniums are the main ionic defects. Channelling experiments have detected interstitial ions occupying *c*-axis tunnels in the rutile structure [18], and the chemical diffusion data in non-stoichiometric rutile have been interpreted in terms of mobile $Ti_i^{\cdot\cdot\cdot}$ defects [19]. Data supporting the presence of oxygen vacancies are more equivocal, though the electrical conductivity data of Iguchi and Yajima [20, 21] have been interpreted in terms of an oxygen vacancy model.

On the basis of the defect equilibria model of Kofstad, the concentration of intrinsic defects in rutile at temperatures below 1700 K and near ambient oxygen fugacities (10^5 Pa) is $< 10^{-3}$ mol %. Since most commercially available rutile crystals contain $> 10^{-3}$ mol % of aliovalent impurities, extrinsic defect concentrations are likely to dominate (see below). For the present hydrothermal experiments, run at the Ni–NiO buffer, the maximum intrinsic departure from stoichiometry occurs at the highest temperature (1373 K), and is of the order of 3×10^{-2} mol %. This is below the concentration (6.6×10^{-2} mol %) of aliovalent impurities in the synthetic crystal used in this study, and thus extrinsic defects are likely to dominate.

4.2.1. Dry gas conditions

The dry gas data at near ambient oxygen fugacities

have readily been interpreted in terms of a vacancy diffusion mechanism in an extrinsic defect regime [2, 5, 9]. Oxygen vacancies are introduced by reactions of the form

$$Al_2O_3 = 2Al_{Ti} + 3O_O^x + V_O^{\cdot\cdot} \quad (9)$$

The corresponding charge neutrality condition is expressed as,

$$[Al_{Ti}] = 2[V_O^{\cdot\cdot}] \quad (10)$$

where square brackets indicate mole fraction concentrations. For a vacancy diffusion mechanism [1]

$$D_{ox} = \gamma a^2 \omega N_v \quad (11)$$

where γ is a geometric factor close to unity, a is the jump distance, ω is the jump attempt frequency and N_v is the vacancy fraction ($\cong [V_O^{\cdot\cdot}]$). From Equations 10 and 11 it is clear that D_{OX} is independent of oxygen activity, as observed by Haul and Dumbgen [5]. Changes in the doping level of the sample will affect the diffusivity only through the vacancy fraction, N_v. Such a trend was observed by Arita *et al.* [9], who reported an increase in D_{OX} upon doping the as-received rutile with Cr_2O_3.

Equation 11 can be written in the standard Arrhenius form [1]

$$D_{ox} = \gamma a^2 \Gamma \exp(\Delta S_v^m/R) \exp(-\Delta H_v^m/RT) N_v \quad (12)$$

where the temperature dependence of ω is defined by the Boltzmann distribution factor $\exp(\Delta S_v^m/R)$. $\exp(-\Delta H_v^m/RT)$, and the pre-exponential constant for vacancy migration is Γ. Since, in this extrinsic region, N_v is the independent of temperature, the empirical activation enthalpy for diffusion, ΔH_D, can be equated directly with that for vacancy migration, ΔH_v^m ($\cong 251$ kJ mol^{-1}).

4.2.2. Hydrothermal conditions

As an initial model for diffusion under hydrothermal conditions we assume that a vacancy diffusion mechanism still dominates and that water dissolves in rutile according to the reaction [5]

$$O_O^x + V_O^{\cdot\cdot} + H_2O = 2OH_O^{\cdot} \quad (13)$$

The substitutional hydroxyl groups are consistent with the available I.R. spectroscopic results [10], and the interpretation of enhanced electronic conductivity in rutile on annealing in hydrogen atmospheres [22]. A similar dissolution mechanism has also been proposed for other non-stoichiometric oxides, e.g. Y_2O_3 and ThO_2 [23–25].

The samples used in this study contain both divalent (Mg) and trivalent (Al, Fe) impurities occurring in similar concentrations. At high hydroxyl levels the charge neutrality condition can, therefore, be expressed as (c.f. Equation 10)

$$2[Mg_{Ti}^{\cdot\cdot}] + [Al_{Ti}^{\prime}] + [Fe_{Ti}^{\prime}] = [OH_o^{\cdot}] \quad (14)$$

where it is assumed that the impurity cations all substitute for Ti. Under this condition the $V_O^{\cdot\cdot}$ concentration is given by

$$[V_O^{\cdot\cdot}] = [OH_O^{\cdot}]^2 f(H_2O)^{-1} K_{13} \quad (15)$$

where K_{13} is the equilibrium constant for Reaction 13. Using this model, at constant temperature, the oxygen vacancy concentration shows a functional dependence on the impurity level and water fugacity as follows

$$V_O^{\cdot\cdot} \alpha ([2Mg_{Ti}^{\cdot\cdot}] + [Al_{Ti}^{\prime}] + [Fe_{Ti}^{\prime}])^2 \quad (16)$$

$$[V_O^{\cdot\cdot}] \alpha f(H_2O)^{-1} \quad (17)$$

Unfortunately, the present work does not include a systematic study of the effect of impurity content and water fugacity on the oxygen diffusivity. However, using the impurity levels reported for the two crystals used in this study, Equation 16 predicts a factor of 16 difference in the diffusion coefficients between the two samples. The measured difference is a factor of 10 (Table I and Fig. 2). Given the limited accuracy of the determinations of impurity concentration and the first order nature of the model, the agreement between theory and experiment is considered to be satisfactory.

Rewriting Equation 12 for the diffusion coefficient and substituting the right hand side of Equation 15 for N_v gives

$$D_{ox} = \gamma a^2 \Gamma \exp(\Delta S_v^m/R) \exp(-\Delta H_v^m/RT) \times [OH_O^{\cdot}]^2 f(H_2O)^{-1} K_{13}^{-1} \quad (18)$$

where the equilibrium constant K_{13} can be written as

$$K_{13} = \exp(\Delta S_{13}/R) \exp(-\Delta H_{13}/RT) \quad (19)$$

Noting that the reciprocal of K_{13} is used in equation 18, the activation enthalpy for diffusion, ΔH_D, is then given by

$$\Delta H_D = \Delta H_v^m - \Delta H_{13} \quad (20)$$

Values for ΔH_D and ΔH_v^m are 170 kJ mol^{-1} (this study) and 251–276 kJ mol^{-1} (dry gas studies [5, 7, 8], respectively. These values yield a solution enthalpy, ΔH_{13}, for water in rutile of 81–106 kJ mol^{-1}. The authors are not aware of any experimental data for the solution enthalpy of water in either rutile or other oxides with which to compare this estimate.

In this study the results have been interpreted within the framework of a simple point defect model. However, given the reduction in the oxygen diffusivity on annealing under hydrothermal conditions it is tempting to speculate on the possible role of shear structures. Reduction of rutile to below the TiO_{2-x} homogeneity range leads to the formation of a series of ordered phases (Magneli phases), with compositions given by Ti_nO_{2n-1} where $n = 4$–53 [26]. Oxygen vacancies in these structures are eliminated by a process of crystallographic shear [27]. Bagshaw and Hyde [28] reported oxygen self-diffusion coefficients for several low-n Magneli phases at 1413 K. Their data are a factor of 5–30 lower than the corresponding results obtained from experiments performed under dry O_2 conditions [5–9] and broadly similar to the present results. The extended shear structures appear to retard oxygen mobility.

Unfortunately, it is difficult to compare directly the results of Bagshaw and Hyde with those that we report here. Their samples are very far from "near

stoichiometry", with compositions in the range $TiO_{1.66}$ to $TiO_{1.83}$. In our samples the maximum intrinsic departure from stoichiometry is only 3×10^{-2} mol%, corresponding to a composition of $TiO_{1.9997}$. No shear structures have been reported in rutiles that are this close to stoichiometric, and hence we strongly favour an interpretation of the data based on point defects.

5. Conclusion

Oxygen self-diffusion co-efficients have been determined in rutile under hydrothermal conditions in the temperature range 873–1373 K. There is a reduced oxygen self-diffusivity compared to existing data for rutile exchanged with dry O_2 at near ambient oxygen fugacities and similar temperatures. The results can be explained by a defect model in which substitutional hydroxyl ions on oxygen lattice sites are the dominant positive defects. The solution reaction may be written as

$$O_O^x + V_O^{\cdot\cdot} + H_2O = 2OH_O^{\cdot} \qquad (21)$$

The solution enthalpy for this reaction lies in the range 81–106 kJ mol^{-1}. At temperatures less than 1400 K and oxygen fugacities greater than the Ni–NiO buffer most commercially available rutile is dominated by extrinsic aliovalent substitutional cations. These cations charge-compensate the substitutional hydroxyl defects. The net effect of this reaction is to reduce the oxygen vacancy concentration and thereby reduce the oxygen self diffusivity.

It is desirable that further experiments are now performed to test this model in detail. In particular, the functional dependency of the diffusion coefficient on the impurity cation content and on the water fugacity should be determined. It is noted, however, that a similar solution mechanism has been proposed to account for the increased electronic conductivity of rutile when annealed in hydrogen [22]. In addition, substitutional hydroxyl ions have been reported to influence the defect chemistry of Y_2O_3 [24], and ThO_2 [25].

References

1. P. KOFSTAD, "Non-stoichiometry, Diffusion and Electrical Conductivity in Binary Metal Oxides" (Wiley, New York, 1972) pp. 139–152.
2. P. KOFSTAD, *J. Less-Common Metals* **13** (1967) 653.
3. F. KROGER, "The Chemistry of Imperfect Crystals" (North Holland Publishing, Amsterdam, 1964) pp. 198–201.
4. R. HAUL and G. DUMBGEN, *Z. Elektrochem.* **66** (1962) 636.
5. R. HAUL and G. DUMBGEN, *J. Phys. Chem. Solids* **26** (1963) 1.
6. R. HAUL, D. JUST and G. DUMBGEN, in "Reactivity of Solids", Proceedings of the 4th International Symposium on the Reactivity of Solids (Elsevier, Amsterdam, 1961) pp. 65–83.
7. D. J. DERRY, D. G. LEES and J. M. CALVERT, *Proc. Brit. Ceram. Soc.* **19** (1971) 77.
8. T. B. GRUENWALD and G. GORDON, *J. Inorg. Nucl. Chem.* **33** (1971) 1151.
9. M. ARITA, M. HOSOYA, M. KOBAYASHI, and M. SOMENO, *J. Amer. Ceram. Soc.* **62** (1979) 443.
10. J. B. BATES and R. A. PERKINS, *Phys. Rev. B* **16** (1977) 3713.
11. J. V. CATHCART, R. A. PERKINS, J. B. BATES and L. C. MANLEY, *J. Appl. Phys.* **50** (1979) 4110.
12. R. FREER and P. F. DENNIS, *Mineral. Mag.* **45** (1982) 197.
13. P. F. DENNIS and R. FREER, in "Non-Stoichiometric Compounds Surfaces, Grain Boundaries and Structural Defects", Vol. 276, edited by J. Nowotny and W. Weppner (NATO ASI. Series C. 1989) pp. 353–362.
14. K. WITTMAACK, in Proceedings of the 8th International Conference on X-ray Optics and Microanalysis (Science, Princeton, NJ, 1979) pp. 32–38.
15. P. F. DENNIS, *J. Geophys. Res.* (red) **89** (1984) 4047.
16. J. CRANK, "The Mathematics of Diffusion" (Oxford University Press, New York, 1975) p. 32.
17. J. W. COLBY, in "Practical Scanning Electron Microscopy", edited by J. I. Goldstein and H. Yakowitz (Plenum, New York, 1975) pp. 529–572.
18. F. YAGI, A. KOYAMA, H. SAKAIRI and R. HASIGUTI, *J. Phys. Soc. Jpn* **42** (1977) 939.
19. N. AIT-YOUNES, F. MILLOT and P. GERDANIA, *Solid State Ionics* **12** (1984) 437.
20. E. IGUCHI and K. YAJIMA, *J. Phys. Soc. Jpn* **32** (1972) 1415.
21. E. IGUCHI and K. YAJIMA, *Trans. Jpn. Inst. Met.* **17** (1972) 45.
22. G. J. HILL, *Brit. J. Appl. Phys.* **1** (1968) 1151.
23. S. STOTZ and C. WAGNER, *Berlin Bunsenges. Physik. Chem.* **70** (1966) 781.
24. T. NORBY and P. KOFSTAD, *J. Amer. Ceram. Soc.* **67** (1984) 786.
25. D. A. SHORES and R. A. RAPP, *J. Electrochem. Soc.* **119** (1972) 300.
26. B. G. HYDE and L. A. BURSILL, in "The Chemistry of Extended Defects in Non-Metallic Solids", edited by L. Eyring and M. O'Keeffe (North-Holland Publishing, Amsterdam, 1970), pp. 347–373.
27. C. R. A. CATLOW, in "Non-Stoichiometric Oxides", edited by O. Toft Sorensen (Academic Press, New York, 1981) pp. 61–98.
28. A. N. BAGSHAW and B. G. HYDE, *J. Phys. Chem. Solids* **37** (1976) 835.

Received 17 November
and accepted 18 December 1992